High-Temperature Spin Crossover in Two Solvent-Free Coordination Polymers with Unusual High Thermal Stability

ARTICLE *in* INORGANIC CHEMISTRY · FEBRUARY 2015

Impact Factor: 4.76 · DOI: 10.1021/acs.inorgchem.5b00119

Inorganic Chemistry

Article

pubs.acs.org/IC

High-Temperature Spin Crossover in Two Solvent-Free Coordination Polymers with Unusual High Thermal Stability

Wei Liu,[†] Xin Bao,[‡] Jin-Yan Li,[†] Yu-Lian Qin,[†] Yan-Cong Chen,[†] Zhao-Ping Ni,*[,†] and Ming-Liang Tong*[,†]

[†]Key Laboratory of Bioinorganic and Synthetic Chemistry of Ministry of Education, School of Chemistry and Chemical Engineering, Sun Yat-Sen University, Guangzhou 510275, People's Republic of China

[‡]Department of Chemistry, School of Chemical Engineering, Nanjing University of Science and Technology, 210094 Nanjing, People's Republic of China

Supporting Information

ABSTRACT: Two solvent-free two-dimensional (2D) coordination polymers, $^{2}_{\infty}$[Fe(ptim)$_2$] (**1**) and $^{2}_{\infty}$[Fe(ptpy)$_2$] (**2**) (Hptim = 2-(5-(4-(1*H*-imidazol-1-yl)phenyl)-4*H*-1,2,4-triazol-3-yl)pyridine; Hptpy = 2-(5-(4-(pyridin-3-yl)phenyl)-4*H*-1,2,4-triazol-3-yl)pyridine), have been successfully prepared by solvothermal reactions. Their iron atoms are bridged by the corresponding multidentate anionic ligands into dense neutral structures. The magnetic data reveal that complexes **1** and **2** are rare examples exhibiting reversible one-step high-temperature spin crossover behaviors with spin transition temperatures of 419 and 416 K, respectively. Moreover, these structures also display remarkable thermal stability up to 714 K (for **1**) and 690 K (for **2**), which are confirmed by thermogravimetric and variable-temperature powder X-ray diffraction analyses.

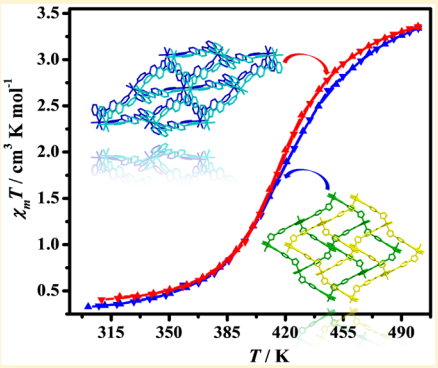

INTRODUCTION

In octahedral transition metal complexes with d^n (n = 4−7) electron configuration, especially the Fe^{II} species, a change of electronic state between low-spin (LS) and high-spin (HS) state can be driven by external perturbations, such as temperature, pressure, light irradiation or pulsed magnetic field.[1] Such a phenomenon is termed "spin crossover" (SCO) or "spin transition" (ST). Due to their potential applications in molecular switches, data storage, and display devices, SCO represents a most spectacular class of bistability in coordination chemistry.[2] Over the past decades, SCO compounds have been intensively investigated.[3] Among them, SCO materials with spin transition temperature ($T_{1/2}$) around room temperature or above are still scarce. In this respect, iron(II) triazole complexes[4] and Hofmann-type networks[5] are promising SCO families with $T_{1/2}$ around room temperature. On the other hand, only a few stable SCO materials above 400 K have been reported.[6] For example, the $T_{1/2}$ of mononuclear compound [Fe(L)](BF$_4$)$_2$ (L = {bis[*N*-(2-pyridylmethyl)-2-aminoethyl]-(2-pyridylmethyl)amine}) can achieve to 455 K.[6b] However, to the best of our knowledge, most reported high-temperature SCO complexes underwent incomplete SCO properties or lost their lattice-solvent molecules without repeatable SCO behaviors after the first heating.[6e,7] Then, the rational design and fabrication of high-temperature SCO property with favorable thermal stability for potential application in extreme conditions is of crucial importance.

Since the main obstacles toward developing high-temperature SCO materials lie in the improper ligand-field strength and poor structural stability caused by the lattice solvents or weak supramolecular interactions, the synthesis of solvent-free and neutral coordination polymer will be a good choice. Recently, by using the polydentate anionic ligands containing a monodentate pyridyl site and a triazol-pyridyl chelating site, we have studied two highly stable neutral 2D coordination polymers, $^{2}_{\infty}$[Fe(L)$_2$] (L = 3-(2-pyridyl)-5-(3-pyridyl)-1,2,4-triazole, (2,3-Hbpt) and 3-(3-methyl-2-pyridyl)-5-(3-pyridyl)-1,2,4-triazole, (2,3-Mebpt)).[6a] They displayed gradual and well-defined two-step SCO behaviors at remarkably high temperatures, namely, Tc_1 = 329 K, Tc_2 = 501 K for $^{2}_{\infty}$[Fe(2,3-bpt)$_2$] and Tc_1 = 351 K, Tc_2 = 520 K for $^{2}_{\infty}$[Fe(2,3-Mebpt)$_2$], which are the highest T_c values reported to date. By using a longer dipyridinyl triazole ligand, 2-(3-(4-(pyridine-4-yl)phenyl)-1H-1,2,4-triazol-5-yl)pyridine (Hpptp), Sun and co-workers also reported a high-temperature SCO polymer, in which about 20% iron(II) was changed into HS state at 390 K for the dehydrated sample.[7e]

Encouraged by the favorable magnetic behavior of $^{2}_{\infty}$[Fe(2,3-Rbpt)$_2$], we modify the ligand skeleton of 2,3-Rbpt for high-temperature SCO species. Here, two new solvent-free neutral coordination polymers, $^{2}_{\infty}$[Fe(ptim)$_2$] (**1**) and $^{2}_{\infty}$[Fe(ptpy)$_2$] (**2**) are synthesized and characterized. The anionic

Received: January 18, 2015

DOI: 10.1021/acs.inorgchem.5b00119
Inorg. Chem. XXXX, XXX, XXX−XXX

ptim$^-$ and ptpy$^-$ ligands can be seen as the extended editions of bpt$^-$ ligand with additional phenyl ring (Scheme 1), which are supposed to maintain its coordination mode to form similar 2D dense structures and enhance the $\pi\cdots\pi$ interactions between layers. Then, two reversible high-temperature SCO materials with enhanced thermal stability are obtained.

Scheme 1. (a) Triazole-based Ligands 2,3-Hbpt, Hptim, and Hptpy; (b) Schematic Representation of the [Fe(ptpy)$_2$] Building Block

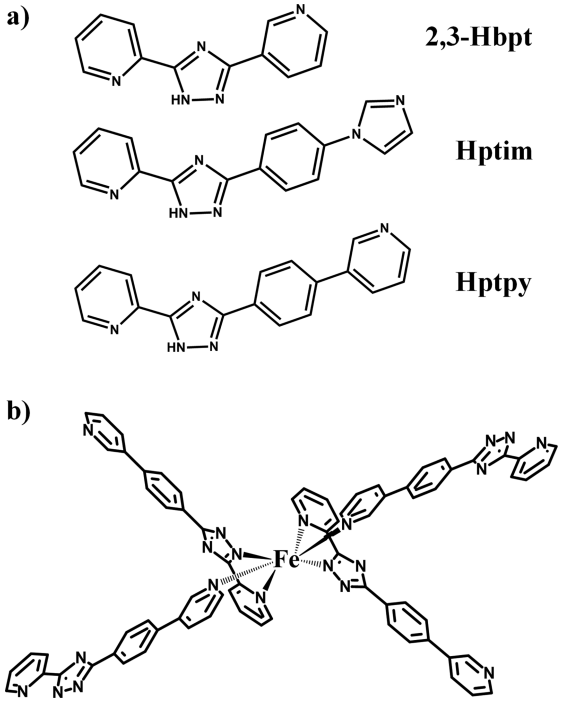

EXPERIMENTAL SECTION

Materials and General Procedures. All the reagents and solvents employed were commercially available and used without further purification.

Caution! *Perchlorate salts are potentially explosive and should be treated with great caution. Only small amounts were used in the present work.*

The VT-PXRD patterns were recorded on a D8 Advance X-ray Diffractometer (Cu Kα, λ= 1.54056 Å) with a high-temperature oven by scanning over the range of 5−50°. Samples were contained in unsealed, thin-walled platinum sheet with an outer diameter of 0.5 mm. The simulated diffraction patterns were generated by Mercury. Infrared spectra were recorded by KBr disc in the range of 4000−400 cm^{-1} with a Bruker-tensor 27 spectrometer. Magnetic susceptibility measurements were carried out by using a superconducting quantum interference device (SQUID) magnetometer (Quantum Design MPMS-XL) under applied magnetic fields of 2T. The samples were sealed in a homemade aluminum foil capsule, mounted inside another homemade aluminum foil bar, and then fixed to the end of the standard sample transport rod. The Pascal's constant was used for the diamagnetic corrections. DSC measurement was performed on a Netzsch DSC 204 instrument under nitrogen atmosphere at a scan rate of 10 K min^{-1} in both heating and cooling modes. The carbon, hydrogen, and nitrogen microanalyses were carried out with an Elementar Vario-ELCHNS elemental analyzer. TG analyses were recorded on a NETZSCH TG209F3 thermoanalyzer by being filled into alumina crucibles under N_2 atmosphere within the temperature range of 300−1050 K at a heating rate of 10 K min^{-1}.

Synthesis. $^2{}_\infty$*[Fe(ptim)$_2$] (1).* A methanol (15 mL) solution of $FeCl_2{\cdot}4H_2O$ (8 mg, 0.04 mmol), Hptim (29 mg, 0.1 mmol), and NaN_3(10 mg, 0.15 mmol) was sealed in a 25 mL Teflon-lined reactor and then heated at 160 °C for 2 days and cooled to room temperature at 5 °C h^{-1}. Dark red rod-like crystals were obtained in 68% yield based on Fe. IR (KBr, cm^{-1}): 3443w, 3113m, 3058w, 1608s, 1562w, 1516s, 1449w, 1420s, 1309w, 1268m, 1239m, 1186m, 1122w, 1062s,

Table 1. Crystallographic Data and Structural Refinement Results for 1−3

	complex					
	1			2		3
formula	$C_{32}H_{22}FeN_{12}$			$C_{36}H_{24}FeN_{10}$		$C_{36}H_{24}CoN_{10}$
FW	630.47			652.50		655.58
temperature, K	298(2)	373(2)	443(2)	298(2)	373(2)	298(2)
crystal system	monoclinic	monoclinic	monoclinic	monoclinic	monoclinic	monoclinic
space group	$P2_1/c$	$P2_1/c$	$P2_1/c$	$P2_1/c$	$P2_1/c$	$P2_1/c$
a, (Å)	8.3518(3)	8.394(4)	8.3756(16)	8.8578(9)	8.834(3)	8.6126(7)
b, (Å)	16.2001(7)	16.315(7)	16.567(3)	8.6866(8)	8.763(3)	8.9163(8)
c, (Å)	11.0557(6)	11.137(6)	11.265(2)	19.5719(17)	19.635(5)	20.0116(15)
β, (deg)	98.357(2)	98.164(15)	98.606(3)	98.141(3)	98.124(6)	96.148(2)
V, (Å)^3	1479.95(12)	1509.6(13)	1545.5(5)	1490.8(2)	1504.7(7)	1527.9(2)
Z	2	2	2	2	2	2
F(000)	648.0	648.0	648.0	672.0	672.0	674.0
ρ_{calcd}, (g cm^{-3})	1.415	1.387	1.355	1.454	1.440	1.425
μ(Mo$_{K\alpha}$), (mm^{-1})	0.555	0.544	0.531	0.552	0.547	0.607
θ range, (deg)	3.13−27.47	3.10−26.37	2.20−26.06	3.15−27.56	3.13−27.34	3.07−27.43
reflns collected	8818	8505	8590	6718	8960	10510
R_{int}	0.0303	0.1221	0.0391	0.0546	0.0694	0.0788
independent reflns	2362	2836	3012	2870	3380	4821
$R_1{}^a$ ($I > 2\sigma(I)$)	0.0348	0.0815	0.0495	0.0588	0.0492	0.0489
$wR_2{}^b$ all data	0.0988	0.2444	0.1332	0.1433	0.1386	0.1199
GOF	1.162	1.025	0.999	1.088	1.064	1.039

$^aR_1 = \sum||F_0| - |F_c||/\sum|F_0|$, $^bwR_2 = [\sum w(F_0^2 - F_c^2)^2/\sum w(F_0^2)^2]^{1/2}$

DOI: 10.1021/acs.inorgchem.5b00119
Inorg. Chem. XXXX, XXX, XXX−XXX

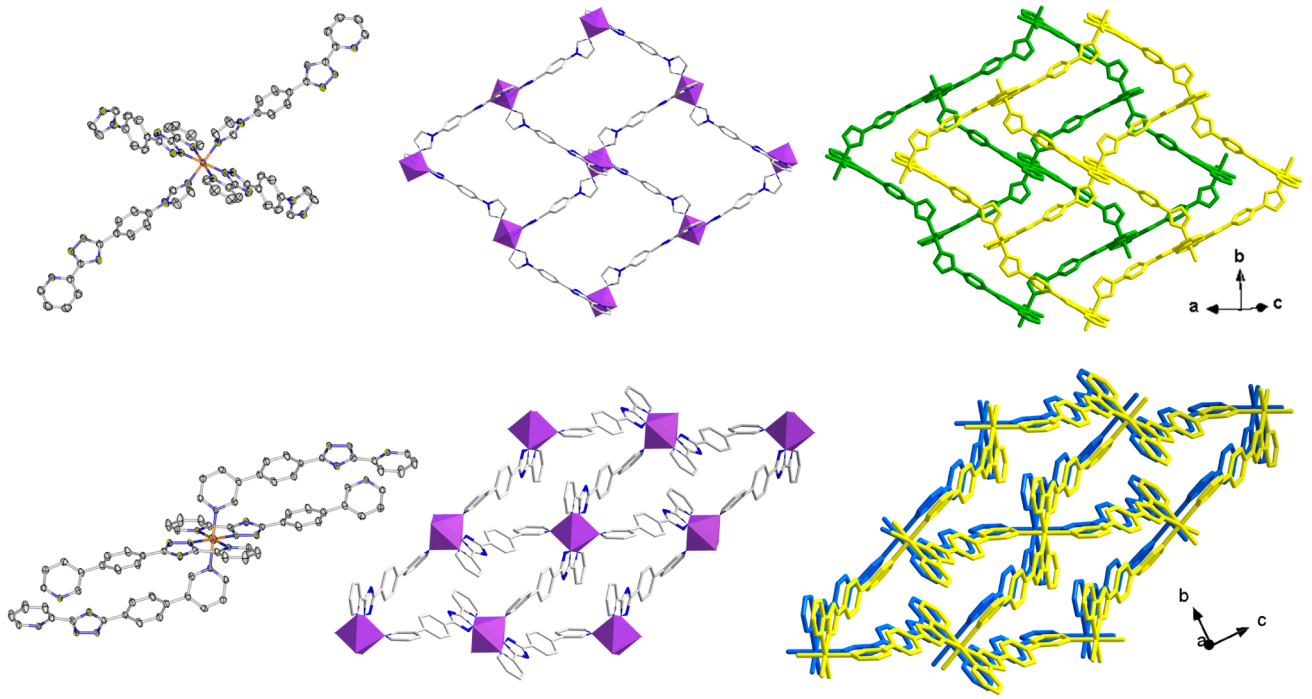

Figure 1. Structure illustrations of (top) **1** and (bottom) **2**: (left) coordination environment of the Fe^{II} atom with thermal ellipsoids at 50% probability; (middle) perspective view of 2D (4,4) rhombic grids; (right) offset packing of two adjacent layers. Color code: (orange) Fe^{II}, (blue) N, (gray) C. Hydrogen atoms have been omitted for clarity.

1027w, 1006m, 965w, 850m, 821m, 791m, 752s, 725s, 668m. Elemental analysis, calcd (%): C, 60.72; H, 3.46; N, 26.21. Found: C, 61.12; H, 3.77; N, 26.08.

*$^2_\infty$[Fe(ptpy)$_2$] (**2**).* A methanol (15 mL) solution of $FeCl_2 \cdot 4H_2O$ (10 mg, 0.05 mmol), Hptpy (30 mg, 0.1 mmol) and triethylamine (10 mg, 0.1 mmol) was sealed in a 25 mL Teflon-lined reactor and then heated at 160 °C for 2 days and cooled to room temperature at 5 °C h^{-1}. Dark red block crystals were obtained in 37% yield based on Fe. IR (KBr, cm^{-1}): 3450m, 3103w, 3061w, 1742w, 1654s, 1419s, 1396s, 1344m, 1291w, 1242w, 1189m, 1140m, 1105m, 1053w, 938m, 852s, 806s, 782m, 747s, 707s. Elemental analysis, calcd (%): C, 66.26; H, 3.70; N, 21.47; found: C, 65.98; H, 3.65; N, 21.38.

*$^2_\infty$[Co(ptpy)$_2$] (**3**).* A mixed solution of methanol (7 mL) and cyclohexane (7 mL) solution of $Co(ClO_4)_2 \cdot 6H_2O$ (40 mg, 0.1 mmol), Hptpy (40 mg, 0.13 mmol) and KSCN (98 mg, 1.0 mmol) was sealed in a 25 mL Teflon-lined reactor and then heated at 180 °C for 2 days and cooled to room temperature at 5 °C h^{-1}. Bright yellow block crystals were obtained in 63% yield based on Fe. IR (KBr, cm^{-1}): 3378s, 3061s, 1652w, 1606s, 1565m, 1513s, 1480m, 1456s, 1448s, 1420s, 1397s, 1345m, 1292m, 1255w, 1191m, 1147m, 1103m, 1028s, 1007s, 853s, 807s, 773w, 752s. Elemental analysis, calcd (%): C, 65.95; H, 3.69; N, 21.36. Found: C, 65.73; H, 3.52; N, 21.03.

Crystal Structure Determination. The diffraction intensity data of **1**−**3** were collected with graphite-monochromated Mo Kα radiation (λ= 0.71073 Å). The intensity data of **1**−**3** at 298(2) and 373(2) K were collected on a Rigaku R-AXIS SPIDER Image Plate diffractometer, while the intensity data of **1** at 443(2) K were collected on a Bruker SMART Apex CCD system apparatus. Absorption corrections were applied upon using multiscan program SADABS.[8] Structures were solved by direct methods. Hydrogen atoms of organic ligands were generated geometrically by the riding mode and all the non-hydrogen atoms were refined anisotropically through full-matrix least-squares technique on F^2 with the SHELXTL program package.[9] Final crystallographic parameters for complexes **1**−**3** are listed in Table 1. Further details are shown in Table S1 (Supporting Information).

CCDC 1043856−1043861 contain the supplementary crystallographic data for this paper. These data can be obtained free of charge from The Cambridge Crystallographic Data Centre via www.ccdc.cam.ac.uk/data_request/cif.

RESULTS AND DISCUSSION

Synthesis and Structure. Solvothermal reaction of the corresponding ligand with stoichiometric amount of $FeCl_2$ produced dark red crystals of $^2_\infty$[Fe(ptim)$_2$] (**1**) and $^2_\infty$[Fe(ptpy)$_2$] (**2**), respectively. When changing $FeCl_2$ into $Co(ClO_4)_2$, complex $^2_\infty$[Co(ptpy)$_2$] (**3**) was obtained. The solvent and ratio of reactants were adjusted respectively to pursue better yields. The final experimental schemes are described in the synthesis section. Chemical formulas of **1**−**3** have been confirmed by single-crystal X-ray diffraction and elemental analysis.

Single crystal X-ray diffraction studies reveal that complexes **1** and **2** crystallize in the monoclinic space group $P2_1/c$ with similar architectures at the applied temperatures (Table 1). At room temperature, the asymmetric unit contains half a Fe^{II} ion and one corresponding ligand. Each Fe^{II} ion is coordinated to six N atoms from four ligands in *trans* configuration to form distorted octahedral geometries, namely, equatorially two triazol-pyridyl chelating sites of two ligands and axially two monodentate imidazolyl (**1**) or pyridyl (**2**) sites from another two ligands (Figure 1). Unlike the bpt^- ligand, $ptim^-$ and $ptpy^-$ ligands are actually noncoplanar (Figure S1, Supporting Information). The dihedral angles of imidazolyl (pyridyl) and phenyl rings to the bidentate part in $ptim^-$ are 83.9 and 25.6° (36.1 and 6.8° in $ptpy^-$), respectively. Connections between Fe^{II} ions and ligands give rise to a 2D [4, 4] rhombic-grids parallel to the [101] plane as shown in Figure 1, in which the neighboring Fe···Fe separations by ligand are 13.3918(4) Å in **1** and 12.9823(8) Å in **2**, respectively.

The 3D close-packed supramolecular structures are formed by interlayer $\pi\cdots\pi$ interactions and C−H···N hydrogen bonds as shown in Figure 2 and Table S1 (Supporting Information).

DOI: 10.1021/acs.inorgchem.5b00119
Inorg. Chem. XXXX, XXX, XXX−XXX

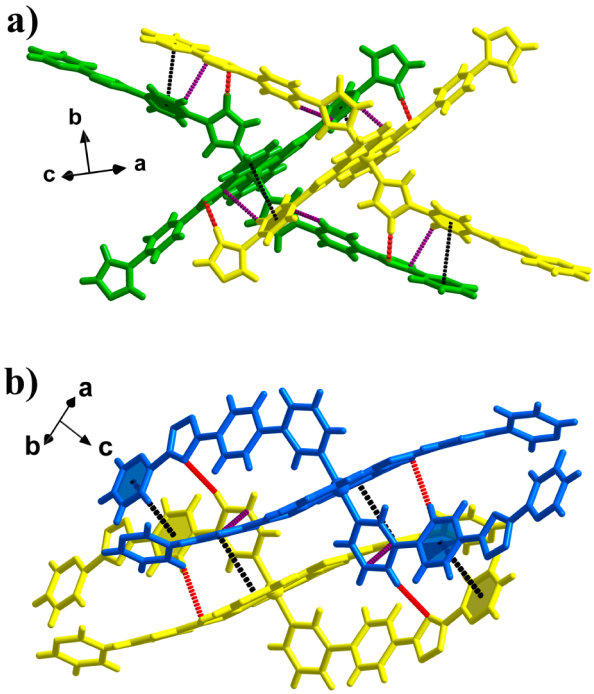

Figure 2. Supramolecular interactions of two adjacent layers: edge-to-face C−H···π, offset face-to-face π···π and hydrogen-bonding interactions are highlighted as purple, black and red dashed sticks, respectively.

In the case of **1**, the additional phenyl ring is involved in three interlayer edge-to-face π···π interactions with the imidazolyl, phenyl, and triazol rings of the neighboring layers while one offset face-to-face π···π interaction with triazol ring. Their C···π distances (Å) /C−H···π angles (deg) are 3.66/126.8, 4.51/141.3, 4.53/147.7 for three edge-to-face π···π interactions. The offset face-to-face π···π distance between the centroids of the aromatic rings is 4.18 Å, while the closest C···C contact is 3.53 Å. Moreover, the intermolecular C−H···N hydrogen bonding (C···N 3.51 Å) between imidazolyl and triazol rings is observed in **1**. The supramolecular structure of **2** is organized by edge-to-face π···π interaction between phenyl and pyridine-3-yl rings (C···π 3.66 Å), offset face-to-face π···π interaction between phenyl and pyridine-2-yl rings (C···C 3.40 Å) and intermolecular C−H···N hydrogen bonding between pyridine-3-yl and triazol rings (C···N 3.69 Å). Obviously, their intermolecular interactions between layers are enhanced when comparing with those of $^{2}_{\infty}$[Fe(2,3-bpt)$_2$] and $^{2}_{\infty}$[Fe(2,3-Mebpt)$_2$].

The occurrence of SCO behavior for **1** can be indicated by the variations of the average Fe−N bond length and octahedral distortion parameter Σ at different temperatures (Table 2). The average Fe−N bond length for **1** is 1.996(2) Å at 298 K, which is consistent with the typical LS Fe−N bond length.[10] It only increaes to 2.012(4) Å upon warming to 373 K. At 443 K, the average Fe−N bond length is 2.115(2) Å, corresponding to the mixture of HS and LS iron atoms. This is also confirmed by the octahedral distortion parameter. The Σ values are 48.2, 49.9 and 58.3° at 298, 373, and 443 K, in accordance with a more distorted octahedral environment for Fe^{II} in HS state. The Fe−N lengths and Σ values for **2** at 298 and 373 K are close to the values of LS Fe^{II}. However, lack of higher temperature structure data prevents us for further investigation.

Magnetic Properties. Variable temperature magnetic susceptibility measurements have been served to monitor the SCO behavior of **1** and **2** directly. It is shown in Figure 3 in the form of $\chi_M T$ versus T plots, where T is the absolute temperature and χ_M is the molar magnetic susceptibility. For complex **1**, the χ_MT value is 0.32 cm^3 K mol^{-1} at 300 K, which is consistent with the value expected for Fe^{II} in LS state. Upon warming, the χ_MT values continuously increase to 3.34 cm^3 K mol^{-1} at 500 K, implying that almost all the Fe^{II} atoms are in the HS states. In the subsequent cooling mode, $\chi_M T$ vs T curve is perfectly reproducible and no thermal hysteresis is observed. Thus, **1** undergoes a reversible one-step SCO behavior with $T_{1/2}$ of about 419 K. The SCO behavior of **2** is highly similar to that of **1** with a tiny lower $T_{1/2}$ value (~416 K).

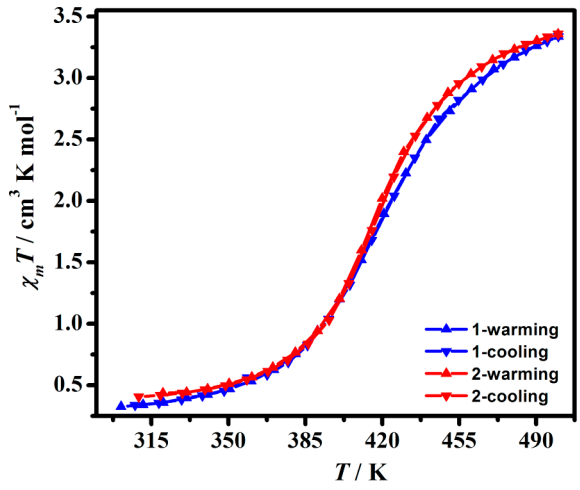

Figure 3. Variable-temperature magnetic susceptibility data of (blue) **1** and (red) **2**.

Thermal Properties. DSC measurements of the two complexes were carried out over the temperature range 300−550 K (Figure 4). For both samples, the DSC curves display only one abnormal peak, culminating at 413 and 417 K for **1**

Table 2. Selected Structural Data for 1 and 2 at Various Temperatures

complex **1**						
temp (K)	Fe−N_{trz}	Fe−N_{py}	Fe−$N_{imi\text{-}end}$	Fe−N_{av}	∑Fe	Fe···Fe distance
298	1.980(2)	2.014(2)	1.994(2)	1.996(2)	48.2	13.3918(4)
373	1.988(4)	2.026(4)	2.021(4)	2.012(4)	49.9	13.4643(39)
443	2.075(2)	2.146(2)	2.124(2)	2.115(2)	58.3	13.5872(15)
complex **2**						
temp (K)	Fe−N_{trz}	Fe−N_{py}	Fe−$N_{py\text{-}end}$	Fe−N_{av}	∑Fe	Fe···Fe distance
298	1.999(3)	2.023(3)	2.015(3)	2.012(3)	42.8	12.9823(8)
373	2.001(3)	2.032(3)	2.031(3)	2.021(3)	47.4	13.0042(25)

DOI: 10.1021/acs.inorgchem.5b00119
Inorg. Chem. XXXX, XXX, XXX−XXX

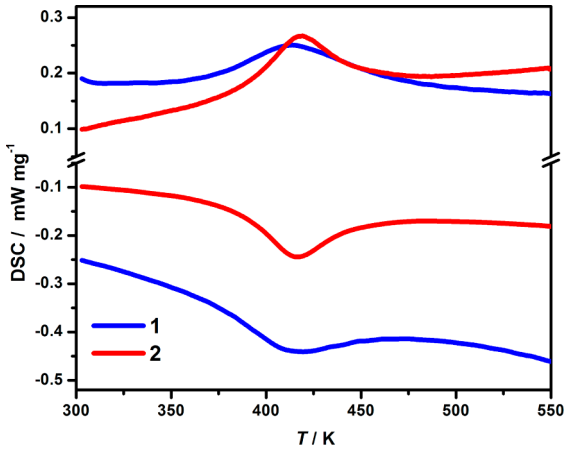

Figure 4. DSC curves for (blue) **1** and (red) **2**.

and **2**, respectively, which are close to the $T_{1/2}$ values from magnetic data. The overall enthalpy (ΔH) and entropy (ΔS) variations are ΔH = 19.8 KJ·mol^{-1}, ΔS = 47.8 J·mol^{-1}·K^{-1} for **1** and ΔH = 24.6 KJ·mol^{-1}, ΔS = 58.7 J·mol^{-1}·K^{-1} for **2**, which are within the experimental range for typical Fe^{II} SCO systems.[11]

The remarkable high thermal stabilities of **1** and **2** are revealed by TG analysis (Figure 5). The samples are heated

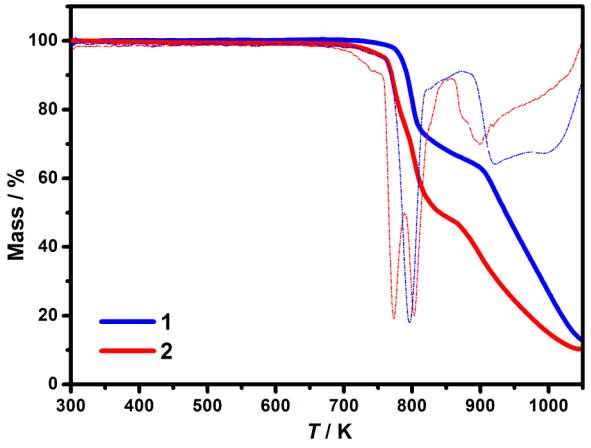

Figure 5. TG Plots for (blue) **1** and (red) **2**.

under N_2 atmosphere and thermally stable up to ~714 and 690 K for **1** and **2**, respectively. Then, their frameworks begin to decompose at higher temperature and accompany obvious exothermic peaks at 797 and 773 K for **1** and **2**, respectively. Since most porous metal−organic frameworks lost their solvents before 473 K and start to degrade after 623 K,[12] the present cases are rare examples with unusually high thermal stabilities promising potential applications in extreme conditions. Their high thermal stability should be benefited from the solvent-free neutral 2D framework. Moreover, the stability temperatures of **1** and **2** are higher than those of our previously reported compounds $^{2}_{\infty}$[Fe(2,3-Hbpt)$_2$] (~670 K) and $^{2}_{\infty}$[Fe(2,3-Mebpt)$_2$] (~634 K). It is assumed that the enhancements of $\pi\cdots\pi$ interactions between layers are responsible for improving their resistance to pyrolysis.

The VT-PXRD patterns were collected for further exploring the thermal stability (Figure 6). The samples show good crystallinities up to 650 K, which is the upper detection limit of

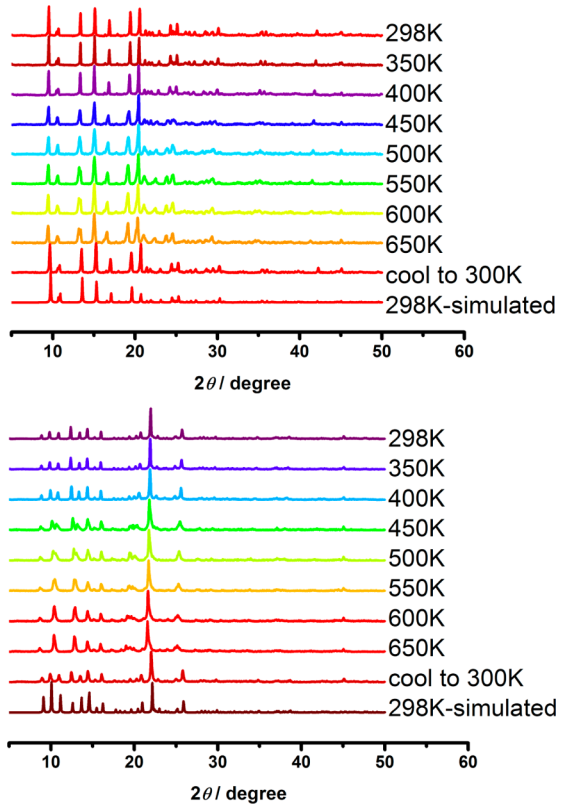

Figure 6. VT-PXRD data as well as the simulated PXRD patterns for (top) **1** and (bottom) **2**.

our measurement. The experimental PXRD patterns of **1** and **2** at 298 K are in good agreement with their simulated data, indicating the phase purities. For **1**, the VT-PXRD patterns remain changeless from 298 to 650 K, further illustrating its high thermal stability. However, in the case of **2**, some diffraction peaks are shifted after heating to 450 K. After cooling from 650 to 300 K, the PXRD pattern can be restored to the original pattern of **2** at 298 K. Thus, the reversible changes of diffraction patterns may be due to the SCO process or temperature-related structural change. To explore it in more detail, an isomorphic cobalt analogue $^{2}_{\infty}$[Co(ptpy)$_2$] (**3**) without SCO behavior is synthesized. Single crystal X-ray analysis shows that **3** is isostructural with **2** at 298 K (Figure S2, Supporting Information). The HS state of Co center is confirmed by the magnetic susceptibility data (Figure S3, Supporting Information), which means that it will keep the same spin state in the range of 298−650 K.[13] As shown in Figure S4 (Supporting Information), the temperature-dependent PXRD patterns for **3** show similar changes to those for **2**, suggesting that the temperature-related structural changes are mainly responsible for the reversible change of PXRD patterns in **2**.

CONCLUSIONS

In summary, we synthesized and characterized two solvent-free neutral 2D coordination polymers. They are rare examples exhibiting reversible one-step high-temperature SCO behaviors. The spin transition temperatures are 419 and 416 K for **1** and **2**, respectively. Moreover, their unusual thermal stabilities are confirmed by TG and VT-PXRD analyses. Their frameworks can be stable up to ~714 and 690 K for **1** and **2**, respectively, which promise potential applications in extreme conditions.

DOI: 10.1021/acs.inorgchem.5b00119
Inorg. Chem. XXXX, XXX, XXX−XXX

Compared with our previous compounds $^{2}_{\infty}[Fe(L)_2]$ (L = 2,3-Hbpt and 2,3-Mebpt), the improvements of thermal stabilities for the present cases should be due to their additional phenyl rings based on the bpt ligand, which enhance the $\pi\cdots\pi$ interactions between layers. Thus, these polydentate anionic ligands for neutral coordination polymers pave the way to construct high-temperature SCO property with unusual high thermal stability.

■ ASSOCIATED CONTENT

Supporting Information

Variable-temperature PXRD measurements, magnetic susceptibility data, diagram showing structure detail of **3**, and selected supramolecular interaction data in **1**, **2** and $[Fe(2,3\text{-bpt})_2]$. This material is available free of charge via the Internet at http://pubs.acs.org.

■ AUTHOR INFORMATION

Corresponding Authors

*E-mail: nizhp@mail.sysu.edu.cn.
*E-mail: tongml@mail.sysu.edu.cn.

Notes

The authors declare no competing financial interest.

■ ACKNOWLEDGMENTS

This work was supported by the NSFC (Grant nos. 91122032, 50872157, 90922009, 21201182, 21373279, and 20821001) and the "973 Project" (2012CB821704).

■ REFERENCES

(1) (a) Murray, K. S. *Spin-Crossover Materials: Properties and Applications* **2013**, 1−54. (b) Halcrow, M. A. *Chem. Soc. Rev.* **2011**, *40*, 4119−4142. (c) Sato, O.; Tao, J.; Zhang, Y. Z. *Angew. Chem., Int. Ed.* **2007**, *46*, 2152−2187. (d) Real, J. A.; Gaspar, A. B.; Munoz, M. C. *Dalton Trans.* **2005**, 2062−2079.

(2) (a) Létard, J.-F.; Guionneau, P.; Goux-Capes, L. Towards spin crossover applications. In *Spin Crossover in Transition Metal Compounds III*; Springer-Verlag: Berlin, 2004; pp 221−249. (b) Bousseksou, A.; Molnár, G.; Salmon, L.; Nicolazzi, W. *Chem. Soc. Rev.* **2011**, *40*, 3313−3335.

(3) Halcrow, M. A. *Spin-Crossover Materials: Properties and Applications*. John Wiley & Sons: Hoboken, NJ, 2013.

(4) (a) Lavrenova, L.; Ikorskii, V.; Varnek, V.; Oglezneva, I.; Larionov, S. *Sov. J. Coordinat. Chem.* **1986**, *12*. (b) Kahn, O.; Martinez, C. J. *Science* **1998**, *279*, 44−48. (c) Krober, J.; Codjovi, E.; Kahn, O.; Groliere, F.; Jay, C. *J. Am. Chem. Soc.* **1993**, *115*, 9810−9811. (d) Coronado, E.; Galán-Mascarós, J. R.; Monrabal-Capilla, M.; García-Martínez, J.; Pardo-Ibáñez, P. *Adv. Mater.* **2007**, *19*, 1359−1361. (e) Bao, X.; Liu, J.-L.; Leng, J.-D.; Lin, Z.; Tong, M.-L.; Nihei, M.; Oshio, H. *Chem.—Eur. J.* **2010**, *16*, 7973−7978. (f) Bao, X.; Guo, P.-H.; Liu, J.-L.; Leng, J.-D.; Tong, M.-L. *Chem.—Eur. J.* **2011**, *17*, 2335−2339. (g) Chen, Y.-C.; Meng, Y.; Ni, Z.-P.; Tong, M.-L. *J. Mater. Chem. C* **2015**, *3*, 945−949.

(5) (a) Niel, V.; Martinez-Agudo, J. M.; Munoz, M. C.; Gaspar, A. B.; Real, J. A. *Inorg. Chem.* **2001**, *40*, 3838−3839. (b) Muñoz, M. C.; Real, J. A. *Coord. Chem. Rev.* **2011**, *255*, 2068−2093. (c) Clements, J. E.; Price, J. R.; Neville, S. M.; Kepert, C. J. *Angew. Chem., Int. Ed.* **2014**, *53*, 10164−10168. (d) Southon, P. D.; Liu, L.; Fellows, E. A.; Price, D. J.; Halder, G. J.; Chapman, K. W.; Moubaraki, B.; Murray, K. S.; Létard, J.-F.; Kepert, C. J. *J. Am. Chem. Soc.* **2009**, *131*, 10998−11009. (e) Bartual-Murgui, C.; Akou, A.; Salmon, L.; Molnár, G.; Thibault, C.; Real, J. A.; Bousseksou, A. *Small* **2011**, *7*, 3385−3391. (f) Bartual-Murgui, C.; Ortega-Villar, N. A.; Shepherd, H. J.; Muñoz, M. C.; Salmon, L.; Molnár, G.; Bousseksou, A.; Real, J. A. *J. Mater. Chem.* **2011**, *21*, 7217−7222. (g) Bao, X.; Shepherd, H. J.; Salmon, L.; Molnár, G.; Tong, M.-L.; Bousseksou, A. *Angew. Chem., Int. Ed.* **2013**, *52*, 1198−1202. (h) Li, J.-Y.; Chen, Y.-C.; Zhang, Z.-M.; Liu, W.; Ni, Z.-P.; Tong, M.-L. *Chem.—Eur. J.* **2015**, *21*, 1645−1651. (i) Li, J.-Y.; Yan, Z.; Ni, Z.-P.; Zhang, Z.-M.; Chen, Y.-C.; Liu, W.; Tong, M.-L. *Inorg. Chem.* **2014**, *53*, 4039−4046. (j) Li, J.-Y.; Ni, Z.-P.; Yan, Z.; Zhang, Z.-M.; Chen, Y.-C.; Liu, W.; Tong, M.-L. *CrystEngComm* **2014**, *16*, 6444−6449.

(6) (a) Bao, X.; Guo, P.-H.; Liu, W.; Tucek, J.; Zhang, W.-X.; Leng, J.-D.; Chen, X.-M.; Gural'skiy, I. y.; Salmon, L.; Bousseksou, A. *Chem. Sci.* **2012**, *3*, 1629−1633. (b) Matouzenko, G. S.; Borshch, S. A.; Jeanneau, E.; Bushuev, M. B. *Chem.—Eur. J.* **2009**, *15*, 1252−1260. (c) Boča, R.; Boča, M.; Dlhan, L.; Falk, K.; Fuess, H.; Haase, W.; Jaroščiak, R.; Papankova, B.; Renz, F.; Vrbova, M. *Inorg. Chem.* **2001**, *40*, 3025−3033. (d) Šalitroš, I.; Pavlik, J.; Boča, R.; Fuhr, O.; Rajadurai, C.; Ruben, M. *CrystEngComm* **2010**, *12*, 2361−2368. (e) Schwarz, G.; Bodenthin, Y.; Tomkowicz, Z.; Haase, W.; Geue, T.; Kohlbrecher, J.; Pietsch, U.; Kurth, D. G. *J. Am. Chem. Soc.* **2011**, *133*, 547−558. (f) Grandjean, F.; Long, G. J.; Hutchinson, B. B.; Ohlhausen, L.; Neill, P.; Holcomb, J. D. *Inorg. Chem.* **1989**, *28*, 4406−4414.

(7) (a) Boča, R.; Renz, F.; Boča, M.; Fuess, H.; Haase, W.; Kickelbick, G.; Linert, W.; Vrbová-Schikora, M. *Inorg. Chem. Commun.* **2005**, *8*, 227−230. (b) Bodenthin, Y.; Schwarz, G.; Tomkowicz, Z.; Nefedov, A.; Lommel, M.; Möhwald, H.; Haase, W.; Kurth, D.; Pietsch, U. *Phys. Rev. B* **2007**, *76*, 064422. (c) Mishra, V.; Mishra, H.; Mukherjee, R.; Codjovi, E.; Linarès, J.; Létard, J.-F.; Desplanches, C.; Baldé, C.; Enachescu, C.; Varret, F. *Dalton Trans.* **2009**, *36*, 7462−7472. (d) Chandrasekhar, N.; Chandrasekar, R. *Dalton Trans.* **2010**, *39*, 9872−9878. (e) Zhang, X.-T.; Sun, D.; Li, B.; Fan, L.-M.; Li, B.; Wei, P.-H. *Cryst. Growth Des.* **2012**, *12*, 3845−3848. (f) Cook, C.; Habib, F.; Aharen, T.; Clérac, R.; Hu, A.; Murugesu, M. *Inorg. Chem.* **2013**, *52*, 1825−1831. (g) Palion-Gazda, J.; Świtlicka-Olszewska, A.; Machura, B.; Grancha, T.; Pardo, E.; Lloret, F.; Julve, M. *Inorg. Chem.* **2014**, *53*, 10009−10011. (h) Shakirova, O.; Daletskii, V.; Lavrenova, L.; Varnek, V.; Rudakov, D.; Potkin, V. *J. Struct. Chem.* **2014**, *55*, 45−52.

(8) (a) Blessing, R. H. *Acta Crystallogr.* **1995**, *A51*, 33. (b) Sheldrick, G. M. *SADABS*; University of Gottingen: Gottingen, Germany, 1996.

(9) (a) Sheldrick, G. M. *Acta Crystallogr.* **2008**, *A64*, 112−122. (b) Sheldrick, G. M. *XPREP. Space Group Determination and Reciprocal Space Plots*. Siemens Analytical X-ray Instruments: Madison, WI, 1991.

(10) (a) Gütlich, P.; Garcia, Y.; Goodwin, H. A. *Chem. Soc. Rev.* **2000**, *29*, 419−427. (b) Guionneau, P.; Marchivie, M.; Bravic, G.; Létard, J.-F.; Chasseau, D. *J. Mater. Chem.* **2002**, *12*, 2546−2551. (c) Krivokapic, I.; Zerara, M.; Daku, M. L.; Vargas, A.; Enachescu, C.; Ambrus, C.; Tregenna-Piggott, P.; Amstutz, N.; Krausz, E.; Hauser, A. *Coord. Chem. Rev.* **2007**, *251*, 364−378.

(11) (a) Šalitroš, I.; Madhu, N.; Boča, R.; Pavlik, J.; Ruben, M. *Monatsh. Chem.* **2009**, *140*, 695−733. (b) Halcrow, M. A. *Spin-Crossover Materials: Properties and Applications* **2013**, 147−169.

(12) (a) Xue, D. X.; Lin, J. B.; Zhang, J. P.; Chen, X. M. *CrystEngComm* **2009**, *11*, 183−188. (b) Gao, Q.; Jiang, F. L.; Wu, M. Y.; Huang, Y. G.; Wei, W.; Hong, M. C. *Cryst. Growth Des.* **2010**, *10*, 184−190. (c) Yang, A. H.; Zhao, L. H.; Quan, Y. P.; Gao, H. L.; Cui, J. Z.; Shi, W.; Cheng, P. *Cryst. Growth Des.* **2010**, *10*, 218−223. (d) Pan, L.; Parker, B.; Huang, X.; Olson, D. H.; Lee, J.; Li, J. *J. Am. Chem. Soc.* **2006**, *128*, 4180−4181.

(13) Adler, P.; Wiehl, L.; Meibner, E.; Köhler, C.; Spiering, H.; Gütlich, P. *J. Phys. Chem. Solids* **1987**, *48*, 517−525.

DOI: 10.1021/acs.inorgchem.5b00119
Inorg. Chem. XXXX, XXX, XXX−XXX